Homeostatic Matching and Nonlinear Amplification at Identified Central Synapses

Hokto Kazama and Rachel I. Wilson

SUPPLEMENTAL EXPERIMENTAL PROCEDURES

Stimulation of ORN axons

Except for the recordings in Figure 1, a minimal stimulation protocol was used throughout the study to stimulate only one ORN axon that was directly presynaptic to the recorded PN. Stimulus intensity was gradually increased from a low level until an EPSC suddenly appeared in an all-or-none manner. Once recruited, the range of stimulus intensities that reliably elicited EPSCs of that size was determined. The cell was discarded unless (1) the average uEPSC amplitude was independent of stimulus intensity over a range of ±5% from the stimulus intensity used to gather data, (2) the onset time of the uEPSC was constant (SD < 0.4 ms), (3) the kinetics of the uEPSC were stable over time, and (4) the rate of axon recruitment failure was less than 10%. A failure to recruit an axon presynaptic to the recorded cell was evidenced by the complete absence of the fast EPSC component. This all-or-nothing failure is extremely unlikely to represent a failure of synaptic transmission at the axon terminal, because when the EPSC does not fail the *CV* of amplitude fluctuations is small, indicating that many vesicles are reliably released onto each PN in response to a single presynaptic spike at these synapses (see Figures 5-7). During repetitive nerve stimulation at high-frequency (50–200 Hz), it is difficult to discriminate between successful and unsuccessful axon recruitment, especially toward the end of the stimulation period. However, we confirmed that axon recruitment failure is not occurring for every stimulation during the train, and thus cannot explain the strong short-term depression we observe (Figure S8). In general, the range of stimulus intensities that elicited reliable EPSCs was ±10% of the intensity used to gather data. On average, ~ 30% of patched cells fulfilled all of the four criteria listed above. The major factors in determining whether a cell met these criteria seemed to be the mechanical stability of the contact between the nerve and the suction electrode as well as the amount of the nerve drawn into the electrode. We also discarded several recordings where the slow component of the evoked EPSC was large relative to the fast component (presumably because we recruited many ORNs presynaptic to other glomeruli before recruiting the first

1

fiber presynaptic to our recorded PN). Once a stable recording was achieved, the nerve was stimulated every 30 s to collect 20–100 (average 35) uEPSCs.

Data analysis

Multiple-probability fluctuation analysis. To measure the mean (I) and the variance (σ^2) of uEPSC amplitudes, current traces were baselined at a time just before the stimulation, and the amplitude was calculated over a 0.6-ms period around the peak of the synaptic response. When we increased the concentration of Cd^{2+} in the saline perfusate, uEPSCs usually stabilized at a lower amplitude within 2-3 minutes, but we always discarded the first 5 minutes of uEPSCs after a saline change in order to maximize stability during each epoch of analysis. Nevertheless, we observed a gradual decrease in uEPSC amplitude during some epochs. Average rundown per epoch was 14.5 ± 2.1 %. This type of rundown has also been reported at other synapses where multiple-probability fluctuation analysis has been applied (Oleskevich et al., 2000; Scheuss et al., 2002). An experiment was discarded if synaptic rundown exceeded 30% during any epoch. To maximize the accuracy of our variance estimates, we computed the variance first within small sets of consecutive recordings and to average these values subsequently (Scheuss and Neher, 2001). Here, the variance of uEPSCs was estimated by averaging the sets of variance values calculated from all possible pairs of consecutive recordings:

$$\sigma^2 = <(I_i - I_{i+1})^2/2> \tag{1}$$

where I_i denotes the ith uEPSC amplitude and pointed brackets $<>$ denote an ensemble average. The variance of background noise was calculated over a 0.6-ms period centered at a time point symmetrical to the peak with respect to the baseline period, and σ^2 was corrected by subtracting this background variance. Assuming that vesicular release follows binomial statistics, then

$$I = Npq \tag{2}$$

$$\sigma^2 = q^2 Np(1 - p) \tag{3}$$

The relationship between I and σ^2 is therefore a parabolic function. To obtain N from I and σ^2, we fitted the variance-mean relationship for each cell with a form of this equation that corrects for variance in q (Silver, 2003):

$$\sigma^2 = (qI - I^2/N)(1 + CV_{II}^2) + qI\,CV_I^2 \qquad (4)$$

where CV_I is the CV of quantal variability at an individual release site and CV_{II} is the CV of quantal variability across release sites. Total variability, which we measured as the CV in mEPSC amplitudes in the same cell (CV_m) is related to CV_I and CV_{II} by (Silver, 2003)

$$CV_m^2 = CV_I^2 + CV_{II}^2 \qquad (5)$$

We assumed an equal contribution of intra- and inter-site variability (after Meyer et al., 2001), and so $CV_I^2 = CV_{II}^2 = (CV_m^2)/2$. Assuming purely intra- or intersite variation produced differences of only $\pm 3\%$ in our estimates of N. The parabolic fit using equation (4) was weighted with the standard deviation of the variance. Equation (2) was then used to calculate p. Figure S4 shows a simulation designed to assess confidence levels for our estimates of synaptic parameters as well as the effects of synaptic rundown.

Measurement of mEPSCs. Miniature EPSCs were detected by searching for events that crossed preset thresholds of the first two time derivatives and also matched the scaled template constructed from typical mEPSCs identified manually (Clements and Bekkers, 1997). Following automatic detection, every event was visually inspected to discard false positive events. Because mEPSCs were small compared to the recording noise, direct measurement of their kinetics was prone to error. For this reason, we smoothed each trace slightly (binomial smooth function in Igor Pro, 5 iterations) before computing amplitude, rise time, and half-decay time. Rise time was calculated as the time elapsed between 10 and 90% of the peak amplitude. The same threshold and template was used for all recordings in all glomeruli. However, the baseline RMS noise of the current trace (measured in 1μM TTX) was higher in PNs with large dendritic arbors. This correlates with the larger membrane capacitance in these PNs (Pearson's $r = 0.84$, $p < 10^{-4}$, $n = 17$ cells, recorded in 1μM TTX). Therefore more mEPSCs might have been rejected in large glomeruli

3

at the stage of template matching, because noise will increase the difference between recorded mEPSCs and the template. This small difference in the "effective" threshold for eEPSC detection may be one reason why we observed a non-significant trend toward a negative correlation between glomerular volume and mEPSC frequency (Pearson's $r = -0.40$, $p = 0.95$, $n = 17$ cells).

Estimation of N and p at a single release probability. Once quantal size (q) is determined in a cell, the number of release sites per single fiber (N) and the probability of release (p) for the synapse can be estimated from equations (2) and (3). We corrected for variability in q by measuring the CV of mEPSC amplitudes and applying equation (4). Although this method can produce estimates that differ substantially from estimates using multiple-probability fluctuation analysis (Sakaba et al., 2002), we found that for the ORN-PN synapses these estimates are in broad agreement.

Analysis of trains (Figure 8G). Binomial statistics indicate that $1/CV^2$ is independent of q.

$$1/CV^2 = I^2/\sigma^2 = Np/(1 - p) \tag{6}$$

Therefore, $1/CV^2$ should remain constant during a train of stimuli if the decrease in uEPSC amplitude is solely due to a change in quantal size. On the other hand, $1/CV^2$ should decrease monotonically with the mean uEPSC amplitude if the synaptic depression is due to a change in the probability of release assuming that the number of release sites does not change over a short period of time (Faber and Korn, 1991).

Image analysis. Confocal sections of the antennal lobe were acquired in 1 μm slices using a Zeiss LSM510 microscope. Images were imported into ImageJ (NIH) for analysis. The volume of a glomerulus was measured using the Measure Stack plugin (B. Dougherty, http://www.optinav.com/imagej.html). The glomerular boundary defined by the nc82 signal was selected as a region of interest (ROI) every 3 slices and these ROIs were interpolated through the stack. The volume of each glomerulus was calculated from this 3D ROI.
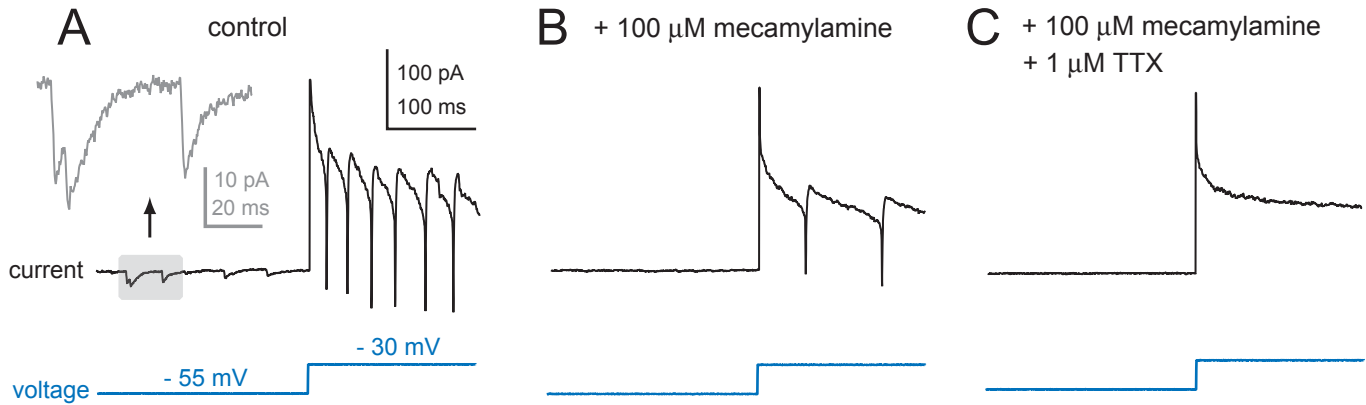
Figure S1

Figure S1. Synaptic currents can be distinguished from currents reflecting the propagation of action potentials.
(A) Recording from a PN in a fly with intact antennae. Because antennae are intact, ORNs are firing action potentials spontaneously. Initial portion of the trace shows spontaneous EPSCs in a PN. Inset shows enlarged EPSCs. Depolarization of the PN to -30 mV triggers a train of large current deflections. These currents are likely to reflect unclamped action potentials in the postsynaptic cell ("action currents"). This is because they are voltage-dependent, and have a large, fast, and stereotyped waveform.
(B) Mecamylamine (a nicotinic antagonist) blocks only spontaneous EPSCs. Depolarization still triggers action currents when synaptic currents are blocked.
(C) Addition of tetrodotoxin (TTX) blocks the presumptive action currents. These results demonstrate that it is possible to record EPSCs from the soma of PNs, and that synaptic currents can be distinguished from action currents. Note that mecamylamine slightly decreases the amplitude and frequency of action currents; this may reflect a change in the efficacy of voltage clamp, or a nonspecific action of the drug.

Note that very small events with EPSC-like kinetics are still observable at high magnification in the presence of TTX when mecamylamine is absent (mEPSC, see Figure 6).
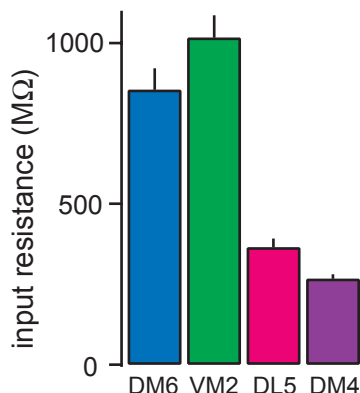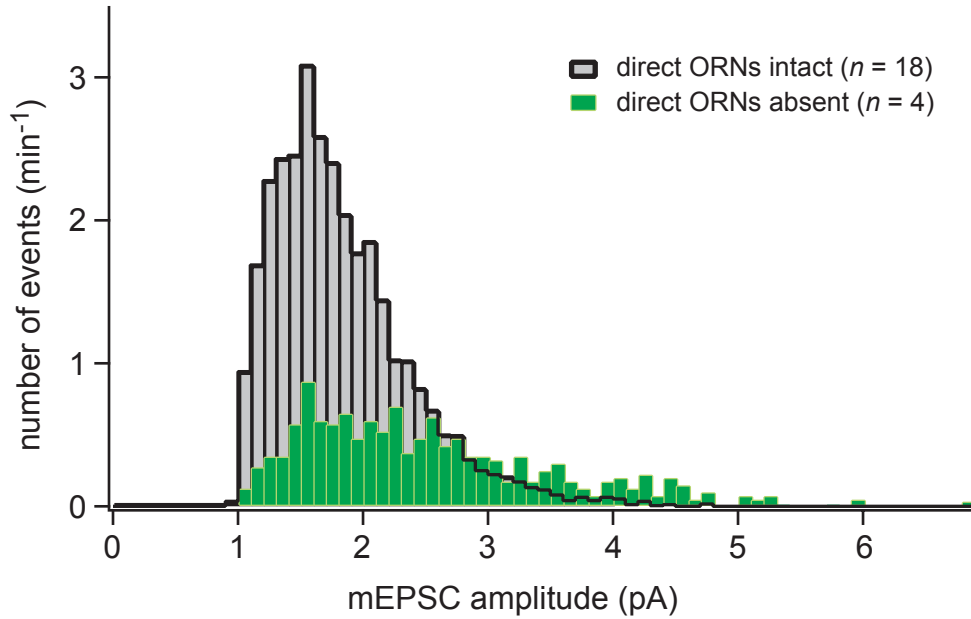
Figure S2

Figure S2. Input resistance measured at the soma.
Input resistance measured at the soma ($R_{input, soma}$) for four different glomeruli (n = 9, 10, 9, and 10 for DM6, VM2, DL5, and DM4). This value differs significantly across glomeruli ($p < 10^{-12}$, ANOVA). Note that $R_{input, soma}$ is smaller for PNs in larger glomeruli (DL5 and DM4) and larger for PNs in smaller glomeruli (DM6 and VM2). This is consistent with the idea that larger dendritic arbors have a lower input resistance due to a larger membrane surface area. Because the soma is some distance away from the dendritic tufts we do not know how $R_{input, soma}$ is related to the input resistance measured at the dendritic compartment ($R_{input, dendrite}$). However, three lines of evidence suggest that $R_{input, soma}$ reflects $R_{input, dendrite}$ to some extent.

First, we have observed that it is possible to detect a change in $R_{input, soma}$ during even a subthreshold odor response. Second, $R_{input, soma}$ is not always correlated with the physical size of the soma. For example, many local interneurons in the antennal lobe have large somata but high $R_{input, soma}$. This suggests that $R_{input, soma}$ is not strictly a reflection of the resistance of somatic membrane. Third, we have performed an experiment where we overexpress an inwardly-rectifying potassium channel that is specifically localized to postsynaptic sites via a PDZ-interacting sequence (Kir2.1, Paradis et al. 2001). When we express this channel in PNs, we observe a significant decrease in $R_{input, soma}$ (301 ± 14 MΩ vs 187 ± 14 MΩ, $p < 0.0005$, t-test, n = 26 and 4). If this channel is indeed localized exclusively to the dendritic tuft, then this result demonstrates that $R_{input, soma}$ is sensitive to manipulations in $R_{input, dendrite}$.

Figure S3

	frequency (Hz)		amplitude (pA)		rise time (ms)		half-decay time (ms)	
	mean	SEM	mean	SEM	mean	SEM	mean	SEM
direct ORNs intact	0.53	0.08	1.71	0.04	1.10	0.02	2.38	0.06
direct ORNs absent	0.23	0.06	2.43	0.11	1.06	0.02	2.26	0.10

Figure S3. Most mEPSCs recorded in PNs are likely to arise from ORN-PN synapses.
Histogram of mEPSC amplitudes recorded in PNs whose direct axonal projections from ORNs are either intact (black bars) or absent (green bars). Note that mEPSC frequency is dramatically decreased when ORN axons are absent.

In experiments where ORN axons remain intact (black), we severed the antennal nerve immediately before our beginning our experiment, leaving ORN axonal projections to the antennal lobe in place. Miniature EPSCs from PNs in glomeruli DM6, VM2, DL5, and DM4.

To completely remove ORN axons from a few glomeruli (green), we removed the maxillary palps 4-7 days before recording. By the end of this period, degeneration of palp ORN axon terminals is complete (Vosshall et al. 2000). We chose to amputate the palps instead of the antennae because the palps contain only ~12% of all ORNs, and so most inputs to the antennal lobe are intact and thus most elements of the antennal lobe circuit (e.g., local interneurons) are likely to be nearly normal. Miniature EPSCs were recorded from PNs in the palp glomerulus VM7.

Interestingly, a population of large mEPSCs appeared after ORN degeneration that was not present in normal glomeruli (compare the right-hand side of these distributions). This might, for example, reflect a potentiation of lateral excitatory connections in response to sensory deprivation.
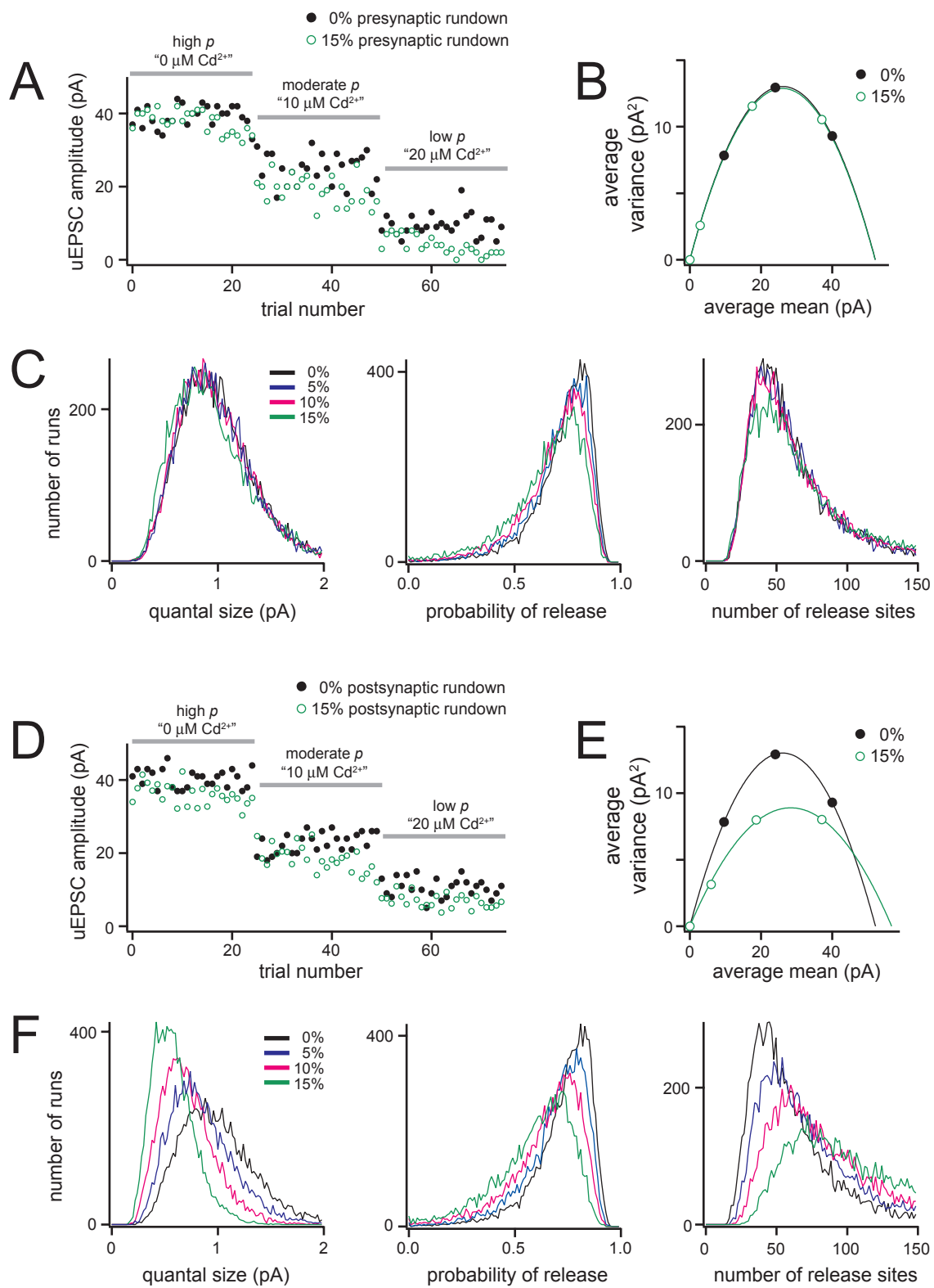
Figure S4

Figure S4. Reliability of the estimates of multiple-probability fluctuation analysis and the effects of synaptic rundown.

The goal of this simple simulation is to examine 1) the confidence level associated with our estimates of synaptic parameters obtained from multiple-probability fluctuation analysis and 2) the effects of pre- or postsynaptic rundown on these estimates. We generated 25 uEPSC amplitudes (the average number of uEPSCs per condition in our actual experiments) for each epoch by simulating binomial vesicular release (panel A, black points). The number of release sites, the initial release probability, and the initial quantal size were set as 50, 0.8, and 1 pA, respectively. Addition of 10 and 20 μM Cd^{2+} was simulated by decreasing release probability by 40 and 60%, respectively. After repeated this simulation 10,000 times with different random seeds, we fitted each variance-mean plot with a parabola (panel B) to obtain 10,000 sets of estimated synaptic parameters. Histograms of these estimates are shown in panel C (black). This represents the confidence levels of our estimates.

Next, we assessed the effect of synaptic rundown on our estimates of synaptic parameters. We repeated the procedure described above, but now with various levels of pre- or postsynaptic rundown (panels A and D, green points). To simulate this rundown, either release probability or quantal size was steadily decreased during the experiment, such that the total rundown during each epoch was 5-15%. The results of these simulations are shown in panel C (presynaptic) and F (postsynaptic). As expected from the binomial model, presynaptic rundown had little effect on our estimates. Because a reduction in p simply shifts the points towards the origin along the variance-mean parabola, the fit of data points with presynaptic rundown will be virtually the same as the fit without rundown (panel B). On the other hand, postsynaptic rundown distorted the shape of the parabola (panel E). This tended to increase the estimated number of release sites (panel F). Estimated release probability was not substantially affected by postsynaptic rundown.
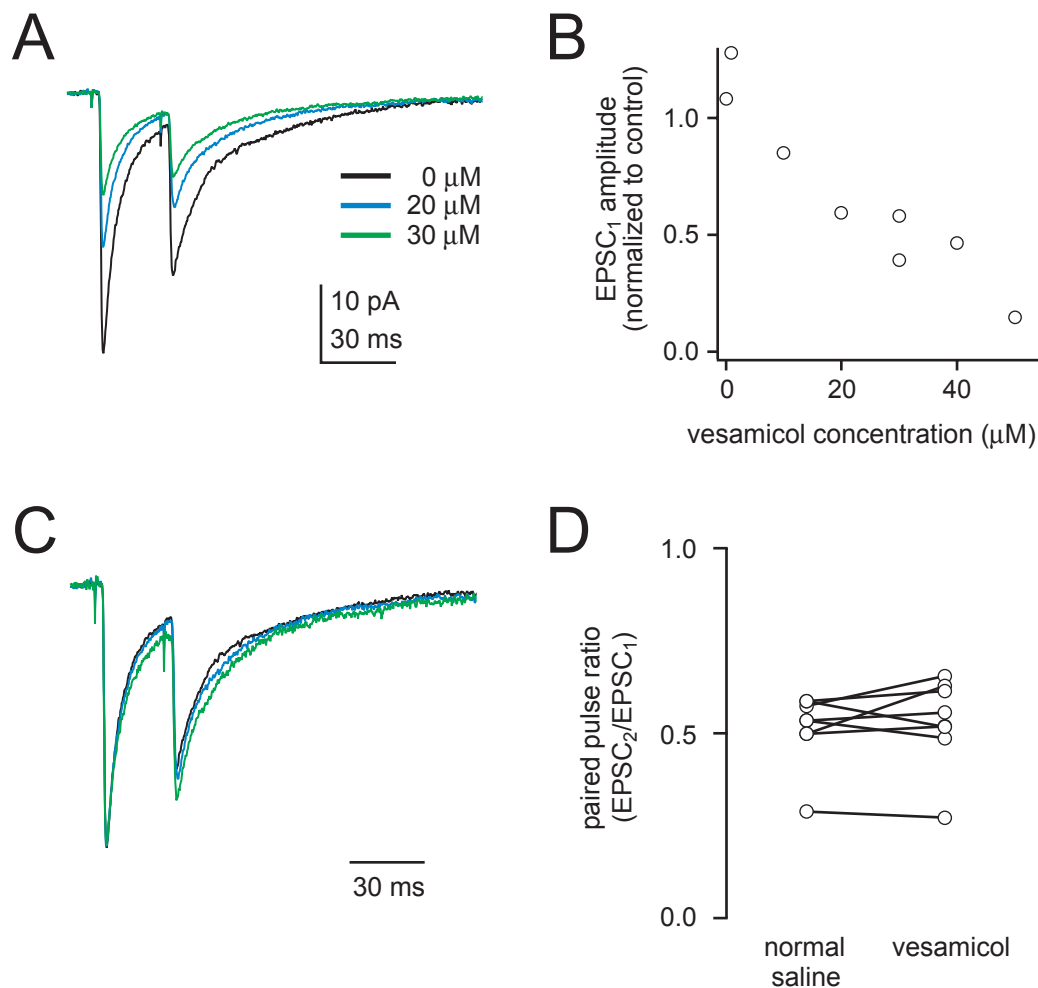
Figure S5

Figure S5. Postsynaptic receptors are not saturated by the acetylcholine released following a single presynaptic spike.
(A) PN response to paired-pulse stimuli (30 ms inter-stimulus interval) recorded in external solution containing 0, 20, or 30 μM vesamicol, an inhibitor of vesicular acetylcholine transporters. All recordings in this figure are from PNs in glomerulus VM2.
(B) The amplitude of the first EPSC decreases with increasing vesamicol concentration, presumably reflecting decreased vesicular filling as vesicular transporters are inhibited (Prior et al., 1992).
(C) Representative traces showing that, for all vesamicol concentrations , the amplitude of the second EPSC is similar when traces in (A) are scaled to the peak of the first EPSC in control solution.
(D) Group data showing that the ratio $EPSC_2/EPSC_1$ does not change in vesamicol
($p > 0.28$, paired t-test, $n = 5$ cells). This result implies that the $EPSC_1$ does not saturate postsynaptic receptors in control solution. (If $EPSC_1$ were saturating, then decreasing vesicular filling should decrease $EPSC_2/EPSC_1$.)
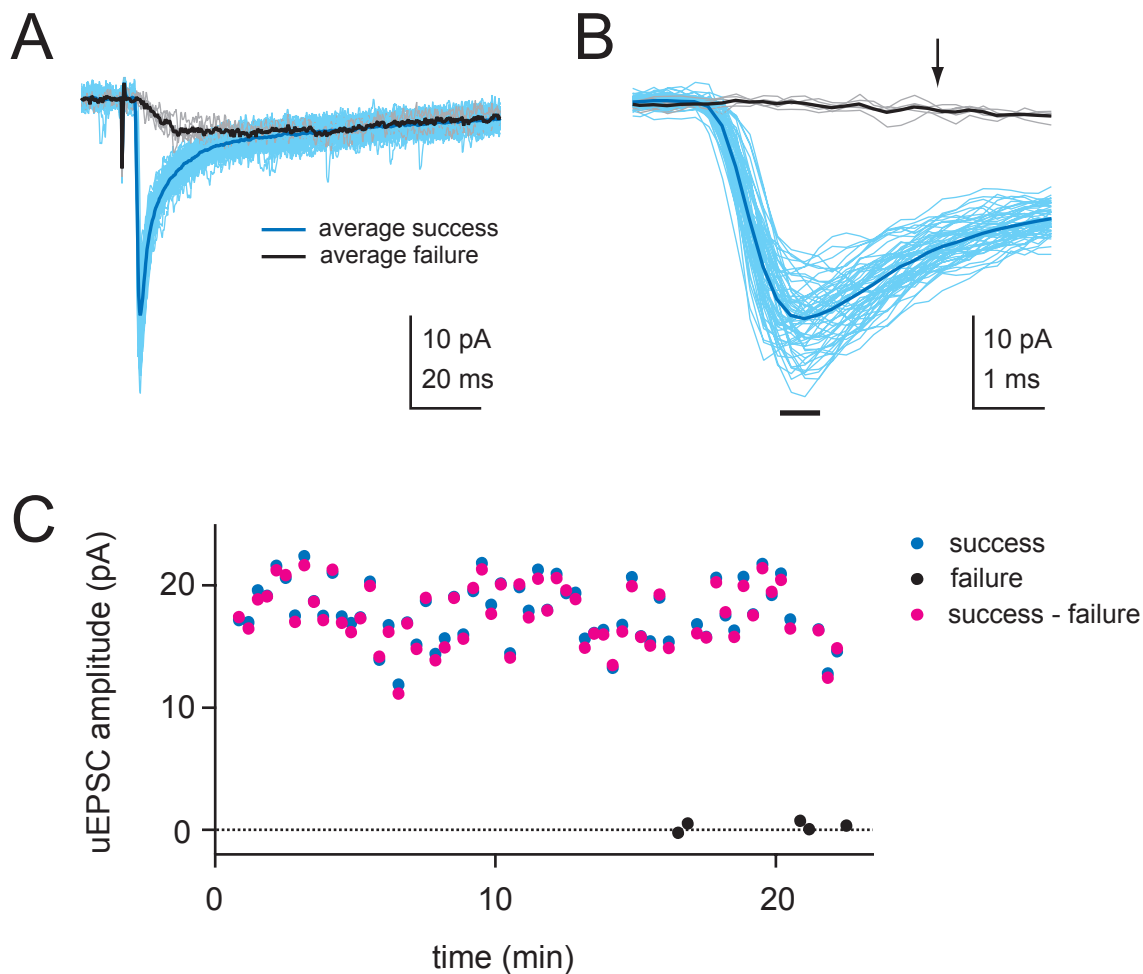
Figure S6

Figure S6. Variability in the size of the lateral component has little effect on the variability in the peak amplitude of the direct component.
(A) Overlay of 61 success and 5 failure traces recorded from a PN postsynaptic to glomerulus DM6 in response to antennal nerve stimulation. Averages in darker colors. Failures likely represent rare instances when the presynaptic fiber that triggers the direct EPSC was not recruited by the stimulation electrode. In these cases, only the slow (presumably lateral) input to the PN is measured.
(B) Enlarged view of (A). EPSC amplitude was calculated over a 0.6-ms period around the peak indicated by a black bar. An arrow indicates the onset of the lateral component.
(C) Plot of uEPSC amplitude over time. For each success trace, one of the failure traces was randomly chosen and subtracted from that success trace. This subtraction had little effect on the variability in success amplitudes. Estimations of the number of release sites and the probability of release were affected by less than 1% (number of release sites, 0.9%; probability of release, 0.8%). This was true even in experiments associated with a larger lateral component (error was < 2%). This is to be expected considering the delayed onset of the lateral component (arrow in B) relative to the direct component (~ 2 ms) and the time to peak of direct components (< 2 ms). Thus, multiple-probability fluctuation analysis is not substantially contaminated by the variable recruitment of lateral inputs.
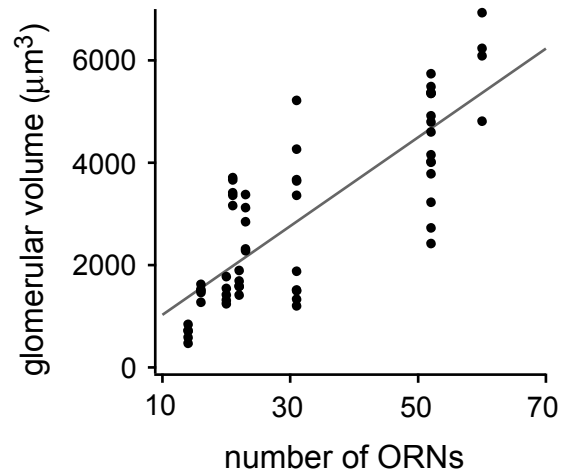
Figure S7

Figure S7. Glomerular volume scales with the number of ORNs.
Glomerular volume is correlated with the number of ORNs presynaptic to each glomerulus (Pearson's $r = 0.81$, $p < 10^{-4}$, $n = 5$ brains×12 glomeruli: DM1, DM2, DM3, DM4, DM5, DA1, DA3, DL5, VA2, VA4, VA5, and V). Gray line is a linear fit. Values on x-axis are taken from Shanbhag et al. (1999) and de Bruyne et al. (1999; 2001). All data are from female flies.
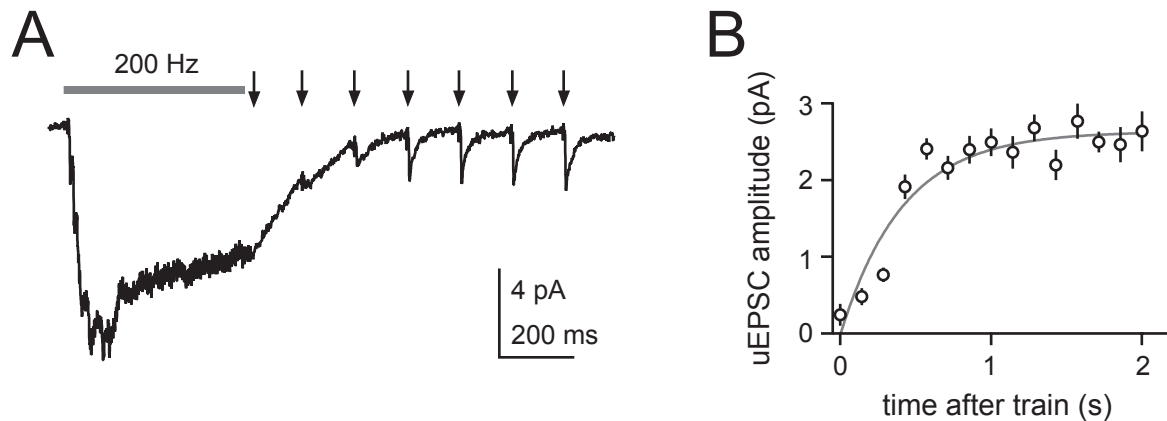
Figure S8

Figure S8. The recovery rate of uEPSC amplitudes following high-frequency stimulation or pause.
 (A) Unitary EPSCs evoked by antennal nerve stimulation mimicking strong odor-evoked input (200 Hz, 500 ms, gray bar). All recordings in (A)-(D) are from PNs in glomerulus VM2.
(B) Recovery rate of uEPSC amplitude following trains of antennal nerve stimulation delivered at 50–200 Hz. Gray curve is an exponential fit. The gradual recovery of uEPSC amplitudes following the high-frequency train demonstrates that axon recruitment failure (which would be all-or-none) cannot explain the depression in the postsynaptic response to the train.
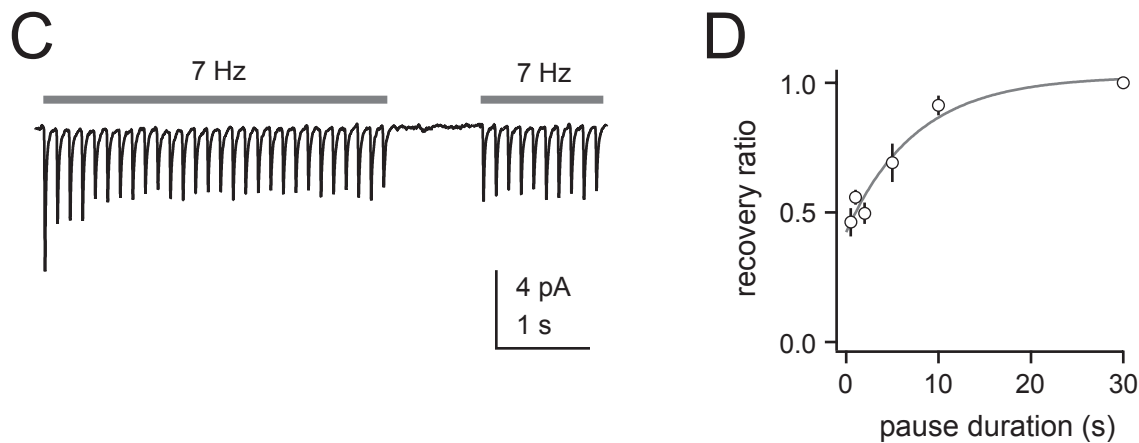
(C) Unitary EPSCs evoked by antennal nerve stimulation at 7 Hz before and after a pause to examine the speed of recovery from synaptic depression caused by spontaneous ORN firing rates.
(D) Recovery rate of uEPSC amplitude is slow (time constant = 7.5 s). Gray curve is an exponential fit. This suggests that the recovery of uEPSC amplitude likely does not account for odor-offset PN excitation in response to odors that suppress activity in the direct ORN inputs to those PNs (see, for example, odor-offset excitation in Schlief and Wilson (2007), Figure 5d).

References

Clements, J. D., and Bekkers, J. M. (1997). Detection of spontaneous synaptic events with an optimally scaled template. Biophysical Journal *73*, 220-229.

Faber, D. S., and Korn, H. (1991). Applicability of the coefficient of variation method for analyzing synaptic plasticity. Biophysical Journal *60*, 1288-1294.

Meyer, A. C., Neher, E., and Schneggenburger, R. (2001). Estimation of quantal size and number of functional active zones at the calyx of held synapse by nonstationary EPSC variance analysis. J Neurosci *21*, 7889-7900.

Oleskevich, S., Clements, J., and Walmsley, B. (2000). Release probability modulates short-term plasticity at a rat giant terminal. J Physiol *524*, 513-523.

Prior, C., Marshall, I. G., and Parsons, S. M. (1992). The pharmacology of vesamicol: an inhibitor of the vesicular acetylcholine transporter. Gen Pharmacol *23*, 1017-1022.

Sakaba, T., Schneggenburger, R., and Neher, E. (2002). Estimation of quantal parameters at the calyx of Held synapse. Neuroscience Research *44*, 343-356.

Scheuss, V., and Neher, E. (2001). Estimating synaptic parameters from mean, variance, and covariance in trains of synaptic responses. Biophysical Journal *81*, 1970-1989.

Scheuss, V., Schneggenburger, R., and Neher, E. (2002). Separation of presynaptic and postsynaptic contributions to depression by covariance analysis of successive EPSCs at the calyx of held synapse. J Neurosci *22*, 728-739.

Schlief, M. L., and Wilson, R. I. (2007). Olfactory processing and behavior downstream from highly selective receptor neurons. Nature Neuroscience *10*, 623-630.

Silver, R. A. (2003). Estimation of nonuniform quantal parameters with multiple-probability fluctuation analysis: theory, application and limitations. Journal of Neuroscience Methods *130*, 127-141.

Vosshall, L. B., Wong, A. M., and Axel, R. (2000). An olfactory sensory map in the fly brain. Cell *102*, 147-159.